

2.1.3 Image analysis by JAXA

JAXA conducted ongoing emergency observations using Daichi in the wake of the Great East Japan Earthquake, releasing reporting of its analysis of eastern Japan and Hokkaido to government ministries and agencies related to disaster management, including the Cabinet Office and local municipalities. The satellite images collected through the Disaster Charter and Sentinel Asia were also analyzed for report to relevant organizations.

The results of the image analysis conducted by JAXA immediately after and after the disaster are outlined here. Support provided by overseas institutions is detailed in Section 2.1.4.

2.1.3.1 Overview of the damage

In view of the difficulty of understanding the extent of the damage from the ground immediately after the disaster, satellite images collected from extensive observations were used to clarify the situation.

JAXA created satellite topographical maps using the data acquired from its emergency observations and previously archived data by superimposing geographical data, and analyzed the disaster areas. The image on the left of Figure 2.1-1 shows a pre-earthquake satellite topographical map based on archived data, while those in the center and on the right show post-earthquake equivalents created by scattering mosaic patterns on AVNIR-2 images taken during emergency observations at around 10:25 JST on March 12 and 10:11 JST on March 14. Figure 2.1-2 shows a disaster area overview produced by AVNIR-2 on March 14.

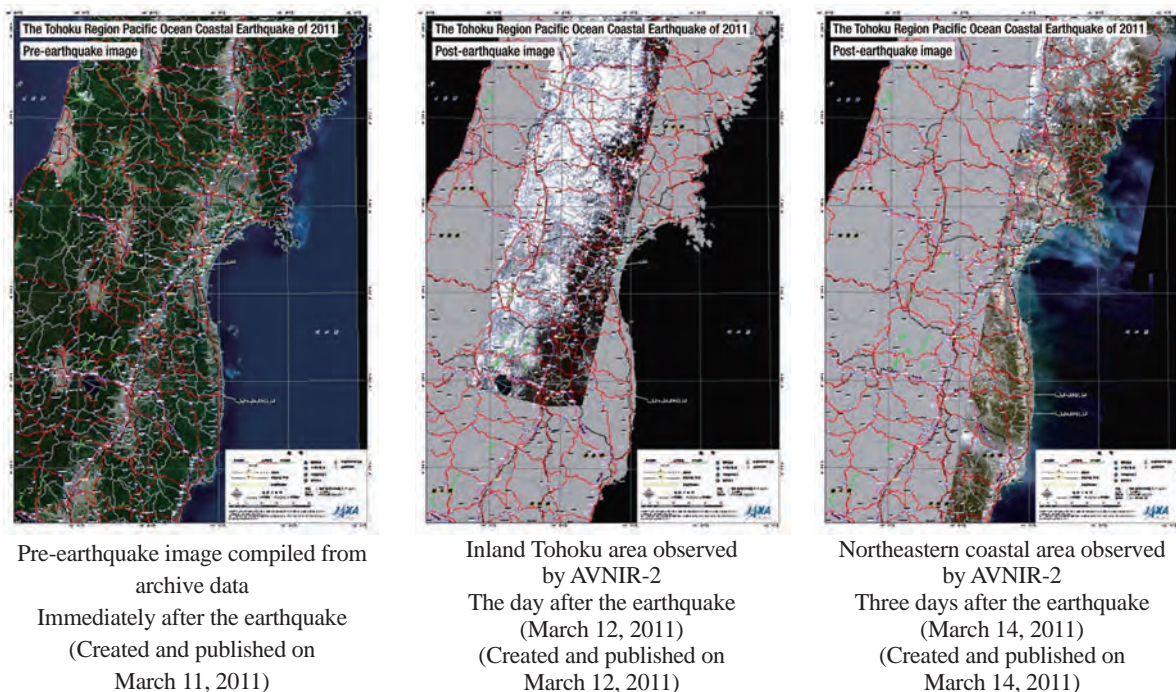


Figure 2.1-1 Pre- and post-disaster satellite topographical maps

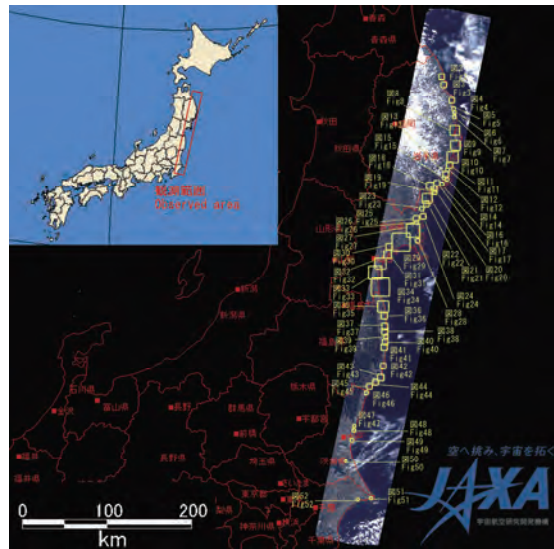


Figure 2.1-2 Overview of the disaster area observed on March 14

2.1.3.2 Analysis of local damage

AVNIR-2 acquired images with minimal cloud on March 14, three days after the disaster, thereby helping to clarify the extent of the damage in Iwate and Miyagi prefectures (the yellow-framed areas in Figure 2.1-2). For example, Figure 2.1-3 shows images of the Omoto area of Iwaizumi Town in Iwate Prefecture enlarged from false-color images produced from a composite of AVNIR-2 band 4, 3 and 2 images from March 14 (after the earthquake) and March 10 (before the earthquake). The clear contrast of areas of vegetation (shown in red) and cloud (white) help to clarify the conditions on the ground. Rice and crop fields are flooded (areas of dark blue after the disaster), and landslides can be seen at the mouth of the river.

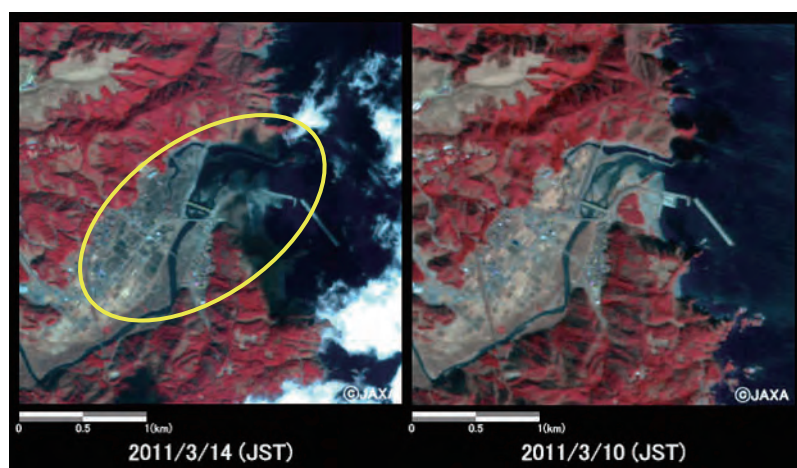


Figure 2.1-3 Flooding in the Omoto area of Iwaizumi Town in Iwate Prefecture (same 3×3 km area)
 Left: after the earthquake (March 14, 2011); right: before the earthquake (March 10, 2011)

Figure 2.1-4 shows enlarged pre- and post-disaster images of Kitaibaraki City in Ibaraki. Clear damage to the sea wall can be seen in the area enclosed in yellow.

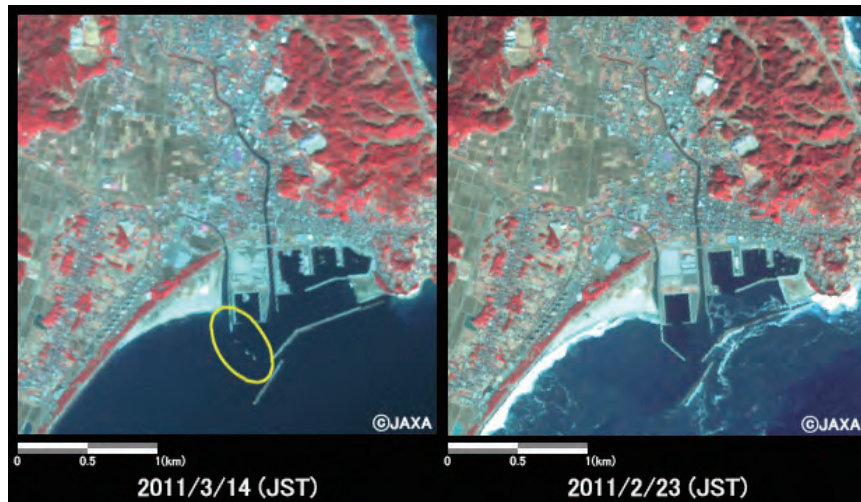


Figure 2.1-4 Kitaibaraki City, Ibaraki (same 3 × 3 km area)

Figure 2.1-5 shows enlarged images of Rokko Bridge in Ibaraki. It can be seen that the middle part of the bridge has collapsed. (Upper part: new bridge under construction)



Figure 2.1-5 Area around Rokko Bridge in Ibaraki (same 1 × 1 km area)

Figure 2.1-6 shows enlarged images of Yawata Town, Iwaki City, Fukushima. Collapsed buildings and other large-scale changes can be seen in the area enclosed in yellow.

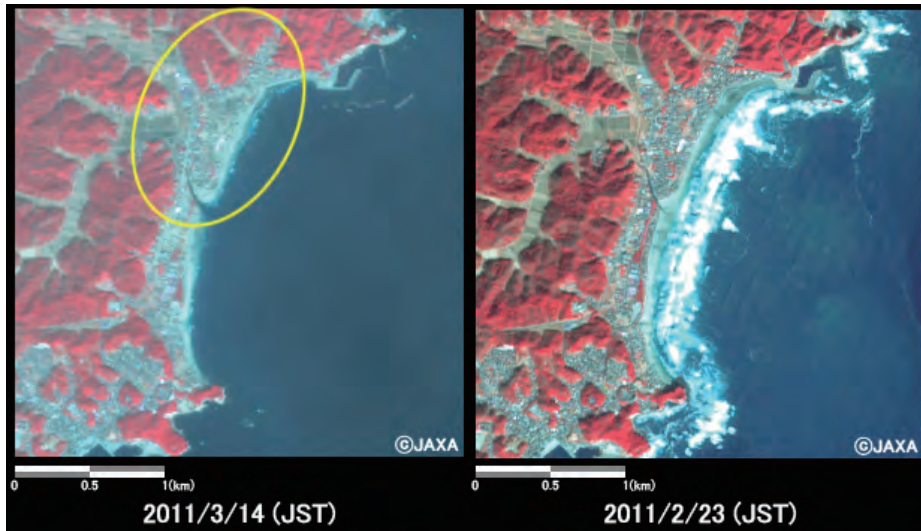


Figure 2.1-6 Yawata Town, Iwaki City, Fukushima (same 3 × 3 km area)

Figures 2.1-7 to 2.1-9 show pre- and post-earthquake bird's-eye views of Rikuzentakata City and Otsuchi Town in the Kamihei area of Iwate created by merging pan-sharpened images from AVNIR-2 and PRISM acquired on March 24, 2011, and November 6, 2010 with Digital Surface Model (DSM) images from PRISM. The images provide a three-dimensional view of the extensive destruction caused by the tsunami to bridges, embankments, urban areas and vegetation.

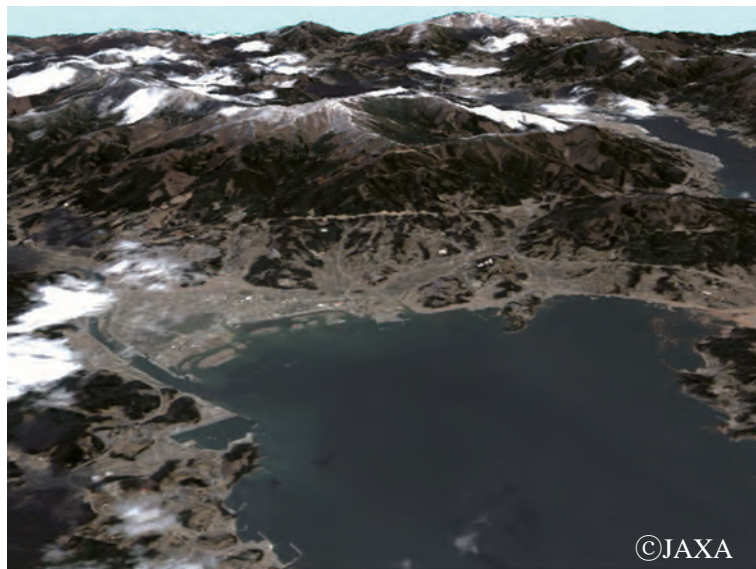


Figure 2.1-7 Post-quake bird's-eye view of the area around Rikuzentakata City, Iwate
(White areas: clouds and snow)



Figure 2.1-8 Pre-quake bird's-eye view of the area around Rikuzentakata City, Iwate

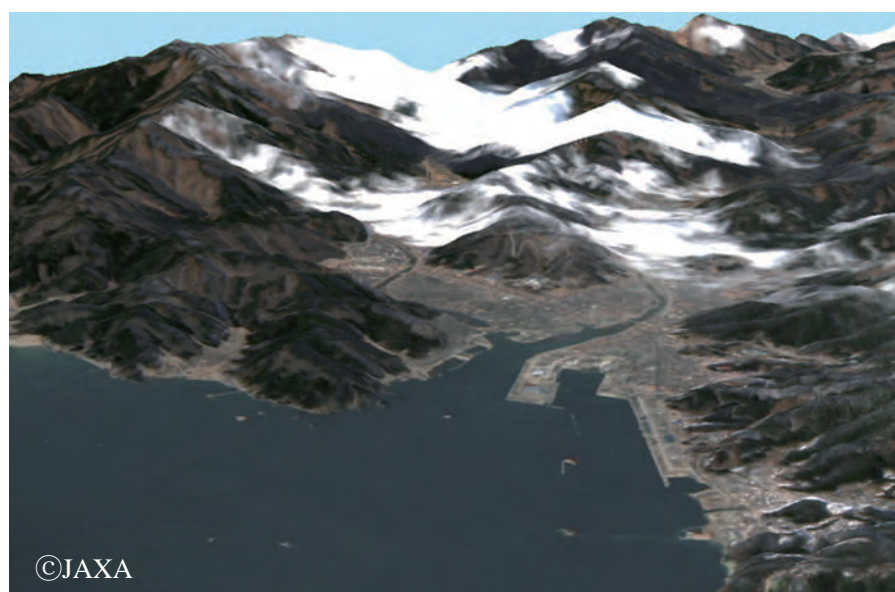


Figure 2.1-9 Post-quake bird's-eye view of the area around Otsuchi Town, Kamihei, Iwate
(White areas: clouds and snow)

2.1.3.3 Landslides

Figure 2.1-10 shows enlarged images of the Oshino district of Nakagawa Town in Tochigi acquired from AVNIR-2 images observed after the earthquake on March 29, 2011 (left), before it on February 27, 2011 (center), and on December 4, 2008 (right). In the area enclosed in yellow, it can be seen that landslides destroyed areas of vegetation and approached buildings to the north.

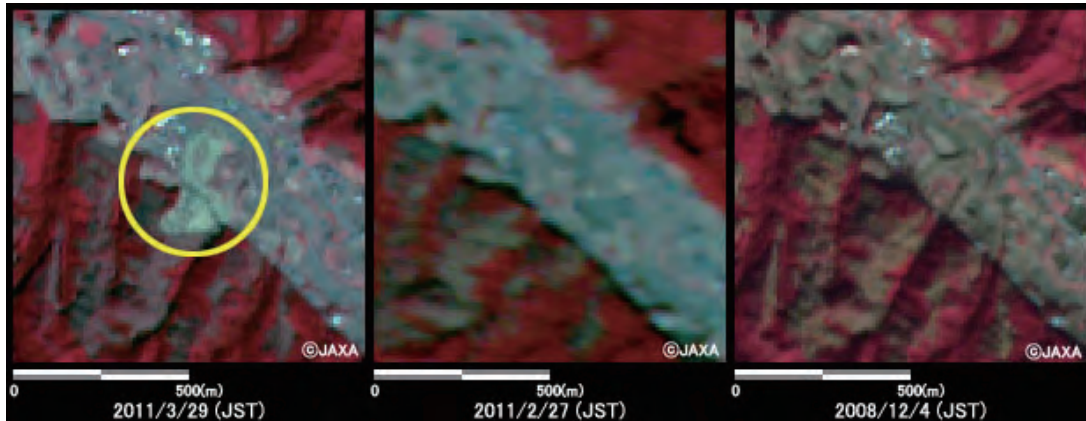


Figure 2.1-10 Oshino district of Nakagawa Town, Tochigi (same 1 × 1 km area)

Figure 2.1-11 shows enlarged images from AVNIR-2 of the area near Lake Fujinuma in Sukagawa City, Fukushima, after the earthquake on March 12 and 29, 2011, and before it on December 4, 2008. In the area enclosed in yellow, it can be seen that the lake burst, sending water into the Taki and Naganuma districts in the lower reaches of the river. It can also be seen that less water was remained in the lake.

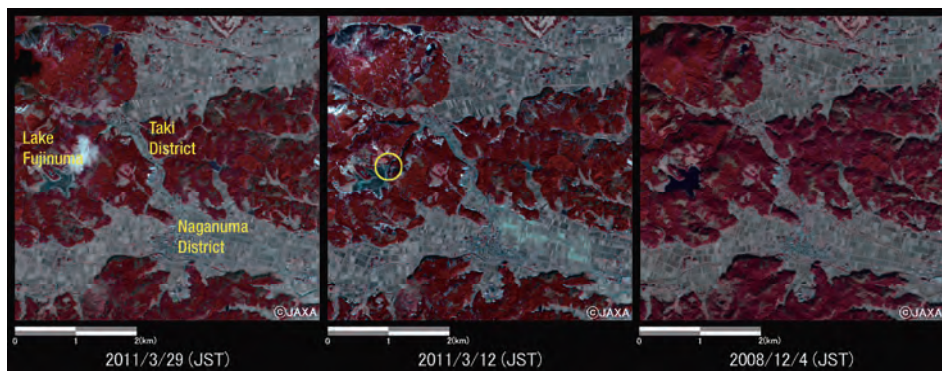


Figure 2.1-11 Area around Lake Fujinuma in Sukagawa City, Fukushima (same 5 × 5 km area)

Left: after the earthquake on March 29, 2011; center: after the earthquake on March 12, 2011; right: before the earthquake on December 4, 2008

Magnitude 7.1 and 6.0 aftershocks occurred in Hamadori, Fukushima, at 17:17 on April 11, triggering landslides at various locations around Iwaki City. Figure 2.1-12 shows enlarged images of a landslide between Iwaki Nakoso IC and Iwaki Yumoto IC on the Joban Expressway taken after the aftershocks on April 12, 2011, and before the aftershocks on April 10, 2011. In the area enclosed in yellow, it can be seen that the landslide reached the expressway.

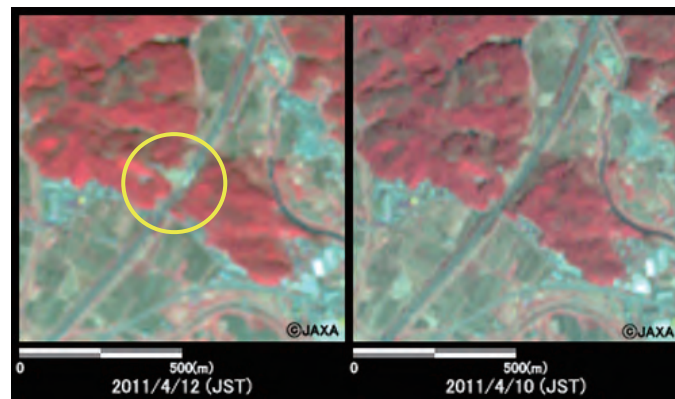


Figure 2.1-12 Joban Expressway in Iwaki City, Fukushima (same 1 × 1 km area)
Left: after the earthquake on April 12, 2011; right: before the earthquake on April 10, 2011

2.1.3.4 Marine debris

Figure 2.1-13 shows enlarged images from AVNIR-2 taken after the earthquake on March 14, 2011 and before it on February 27, 2011, around Aburasaki, Rikuzentakata City, Iwate. It can be seen that a large amount of marine debris washed into the bay and that plains were flooded.

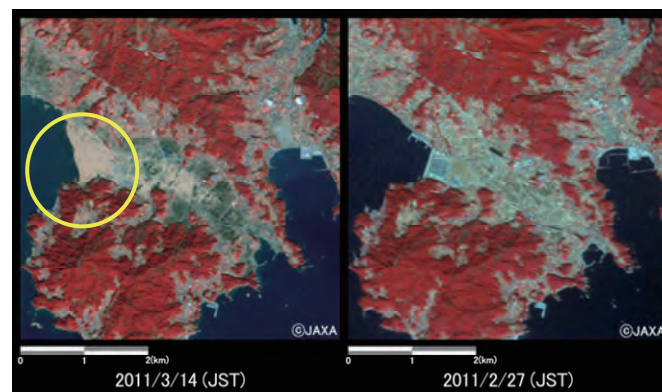


Figure 2.1-13 Aburasaki, Rikuzentakata City, Iwate (same 5 × 5 km area)
Left: after the earthquake on March 14, 2011; right: before the earthquake on February 27, 2011

Figure 2.1-14 shows an image from PALSAR observed around Sendai Bay on March 13. The green circles show debris; roughly 30 objects can be seen. The many white lines extending from north to south are caused by a phenomenon called ambiguity, in which bright land reflects on the dark surface of the sea.

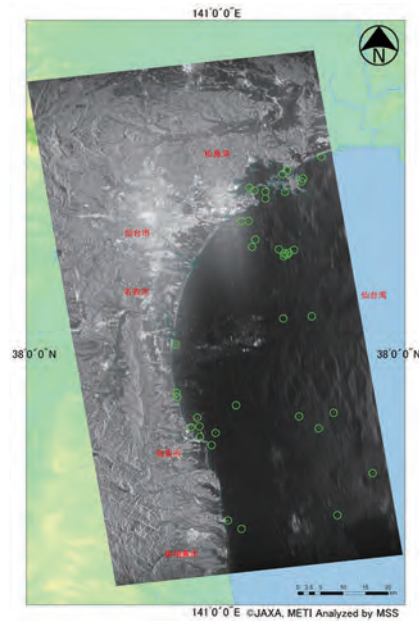


Figure 2.1-14 Marine debris observed by PALSAR (near Sendai Bay)
(around 22:11 on March 13, 2011)

2.1.3.5 Flood damage

Satellite observations are effective in determining the extent of tsunami-related flooding. Figure 2.1-15 shows enlarged pre- and post-earthquake images of the area around the Odaka district of Soma City in Fukushima taken by AVNIR-2 on March 14 and February 23. Areas of vegetation (shown in red) are still present, but extensive flooding is seen in rice fields and other areas of arable fields (shown in dark blue).

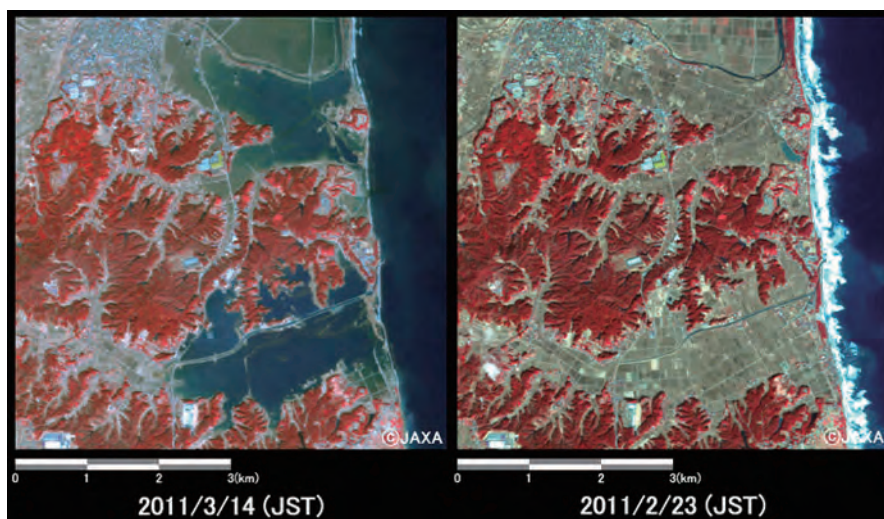


Figure 2.1-15 Flooding around Odaka, Minamisoma City, Fukushima (same 6 × 6 km area)

Observations using PALSAR also help to identify areas of flooding based on the properties of reflection. As shown in Figure 2.1-16, most signals transmitted from the satellite bounce off water when flooding is present, which results in less reflection back toward the satellite and makes terrain appear darker (left). After the floodwater dissipates, signal reflection back to the satellite is increased, making terrain appear lighter (right).

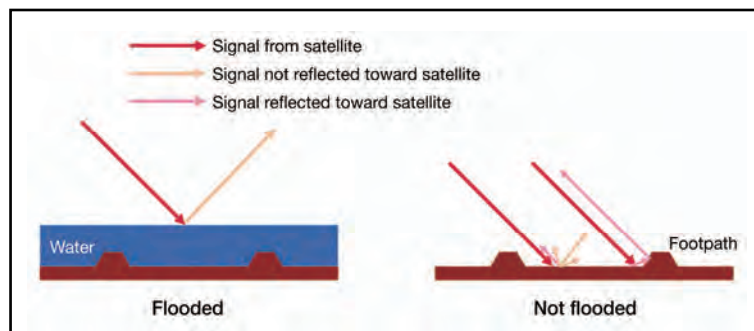


Figure 2.1-16 Difference in signal reflection with and without floodwater

Based on this characteristic, Figure 2.1-7 shows a pseudo-color image from PALSAR consisting of images observed on April 2 (red, incidence angle: 41.4°) and March 16, 2011 (green and blue, incidence angle: 43.4°). The images are merged to highlight changes along the Pacific coast from the Shimokita Peninsula to Chiba.

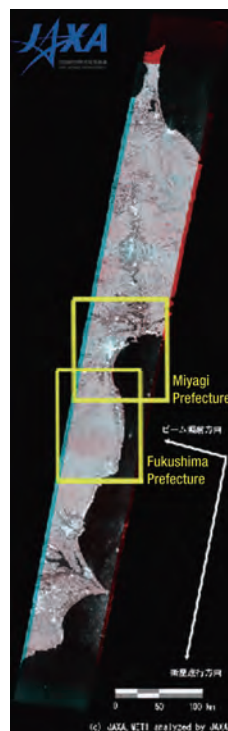


Figure 2.1-17 Pseudo-color PALSAR image

(R: observation on April 2 (incidence angle: 41.4°); G, B: observation on March 16 (incidence angle: 43.4°))

The geographical features of the two pseudo-color images were adjusted to compensate for their different incidence angles. The coastal areas of Miyagi and Fukushima shown in Figure 2.1-17 are enlarged in Figure 2.1-18.

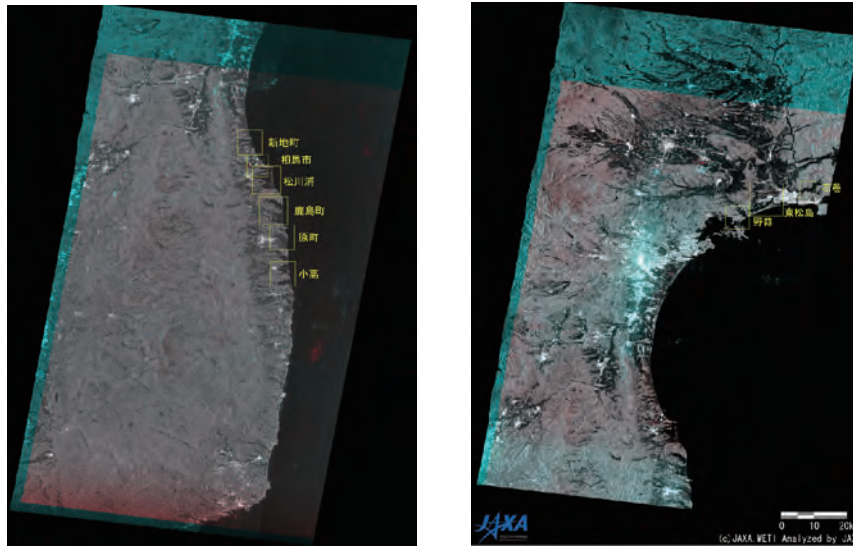


Figure 2.1-18 Enlarged images of coastal areas in Fukushima and Miyagi

Left: coastal area of Fukushima; right: coastal area of Miyagi

Figure 2.1-19 shows an enlarged image of the Ishinomaki area from Figure 2.1-18, which is a part of areas where changes can be seen between the two pseudo-color images shown in Figure 2.1-18 for March 16 and April 2. Areas that are lighter in the former (i.e., those with higher levels of reflection) than in the latter are indicated in blue, while those that are lighter in the latter are shown in red.

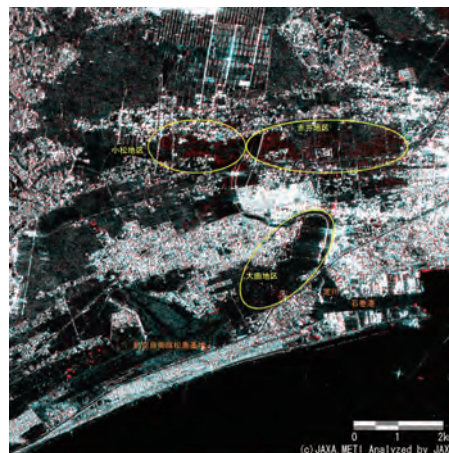


Figure 2.1-19 Enlarged image of the area around Ishinomaki

The rice fields along the Mano River (including those in the districts of Ouri, Negishi and Takaki) look dark due to floodwater, but are all lighter in the April image. This is because the ground surface was exposed as the floodwater dissipated, resulting in increased signal reflection.

Flooded parts of disaster-stricken areas were also detected using AVNIR-2 and PALSAR.

The total area of flooding in each prefecture was determined using pre- and post-earthquake images from AVNIR-2, and the results are shown in Table 2.1-4. Zero is shown for areas where observation was not possible due to clouds and for those where no flooding occurred. The results, classified into municipal government areas, were provided to central government ministries and agencies. By way of example, Figure 2.1-20 shows the results for the cities of Soma and Minamisoma. It can be seen that coastal areas were extensively flooded just after the disaster on March 14, and that the floodwater dissipated over time. Similar analysis was also conducted with images from PALSAR (see Section 2.1.7.2 for the analysis results).

Table 2.1-4 Total areas of flooding by prefecture as observed by AVNIR-2

Name of prefecture	Flooded area [km ²]						
	As of March 14	As of March 19	As of April 5	As of April 12	As of April 17	As of April 20	
	Observation on March 14	Observation on March 19	Observation on April 5	Observation on April 12	Observation on April 17	Observation on April 18	Observation on April 20
Iwate Prefecture	2.74	1.96	1.10	1.03	0.75	0.69	0
Miyagi Prefecture	109.09	64.68	22.28	14.21	7.61	4.28	0
Fukushima Prefecture	25.90	21.52	13.94	11.03	5.85	0	0.09
Ibaraki Prefecture	2.62	0.05	0.10	0.09	0.04	0	0.02
Chiba Prefecture	1.07	0.16	0.02	0	0	0	0.00

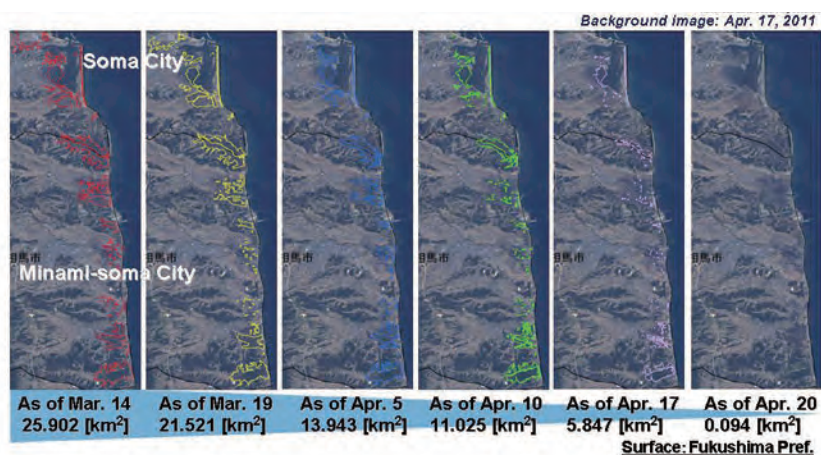


Figure 2.1-20 Results of observation by AVNIR-2 to determine total areas of flooding in the Fukushima cities of Soma and Minamisoma

2.1.3.6 Crustal movement

(a) Detection of crustal movement

Differential interferometric synthetic aperture radar (DInSAR) analysis was performed to detect crustal movement in relation to the Great East Japan Earthquake by comparing pre- and post-earthquake images acquired from the same orbit on April 18 and March 3, 2011.

Crustal deformation considered to have been caused by the M-7.0 earthquake centered on Hamadori in Fukushima on April 11, 2011, was also detected.

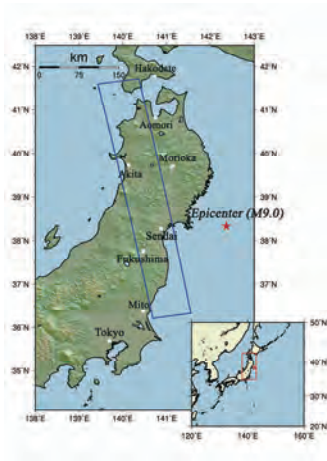


Figure 2.1-21 Range of PALSAR observation to detect crustal movement

SRTM3 data were used to provide digital elevation models. The red star shows the epicenter of the Great East Japan Earthquake.

The image on the left of Figure 2.1-22 was generated from PALSAR data acquired before the disaster (on March 3) and after it (on April 18) using differential interferometric SAR (DInSAR), and the image on the right is from PALSAR observation after the earthquake. Interference fringes (rainbow-color stripes) are seen in most parts of the left DInSAR image, indicating extensive crustal deformation typical of a massive earthquake. Diastrophism resulting in movement of around 2.6 m away from the satellite (including the gaps toward the east) is also seen in coastal areas of Sendai City in the vicinity of the epicenter.

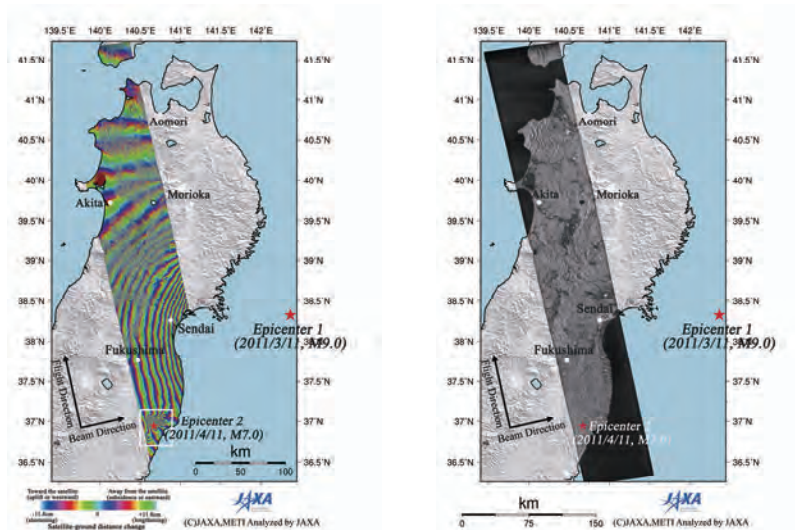


Figure 2.1-22 DInSAR images from PALSAR showing crustal deformation

Left: DInSAR image from PALSAR (crustal deformation). The section in the white frame is enlarged in Figure 2.1-23.

Right: PALSAR image taken after the earthquake. The Epicenter 1 star shows the focal point of the Great East Japan Earthquake (M 9.0), and the Epicenter 2 star shows that of the earthquake centered on Hamadori in Fukushima on April 11, 2011 (M 7.0). (Epicenter 2 data courtesy of the Japan Meteorological Agency)

In Figure 2.1-23, regional interference fringes that differ significantly from those around them can be seen. This is considered to stem from crustal deformation associated with the April 11 2011 Fukushima Hamadori earthquake (M 7.0), which is thought to have caused crustal movement of 2 m or more around the epicenter.

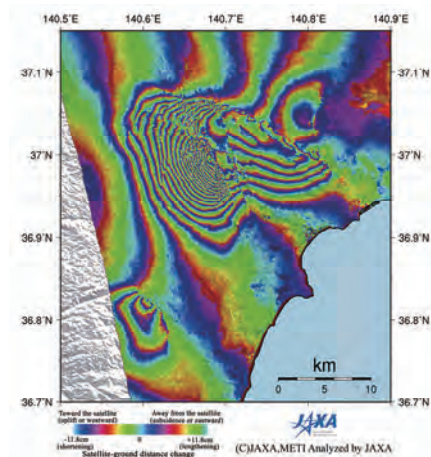


Figure 2.1-23 Enlarged DInSAR image from PALSAR (crustal movement)
(area shown in the white frame in Figure 2.1-22)

2.1.3.7 Liquefaction

Figure 2.1-24 shows enlarged images of the area around Kaihin-Makuhari Station on the Keiyo Line in Chiba based on AVNIR-2 data acquired after the earthquake on March 17, 2011 (left) and before the earthquake on February 23, 2011 (right). The areas circled in yellow show a lighter shade of gray after the earthquake due to liquefaction, which brought moist sand up to the ground surface. An example of this phenomenon is shown in the photo in Figure 2.1-25, taken on March 18, 2011.



Figure 2.1-24 Kaihin-Makuhari Station in Chiba (same 3 × 3 km area)



Figure 2.1-25 Liquefaction in Makuhari Kaihin Park (photo taken on March 18)

Figure 2.1-26 shows the results of liquefaction detection in a high-resolution image of the coastal area between Makuhari Hongo and Makuhari stations taken at 10:57 JST on March 17 2011 by the United States' WorldView-2 satellite, whose data is provided through Disaster Charter.



Figure 2.1-26 Areas of liquefaction between Makuhari Hongo and Makuhari stations

Left: overview; right: enlargement

2.1.3.8 Fire

Figure 2.1-27 shows enlarged pre- and post-earthquake images of the area around an oil refinery in Ichihara City, Chiba, observed by AVNIR-2 on March 17, 2011 (left) and on February 23, 2011 (right).

The black area circled in yellow is the site of a fire caused by the Earthquake.



Figure 2.1-27 Oil refinery in Ichihara City, Chiba (same 3 × 3 km area)

Figure 2.1-28 shows a satellite topographical image in which the area of the fire at the oil refinery can be seen. This is based on an image observed by FORMOSAT-2 on March 13 2011 through Sentinel Asia.

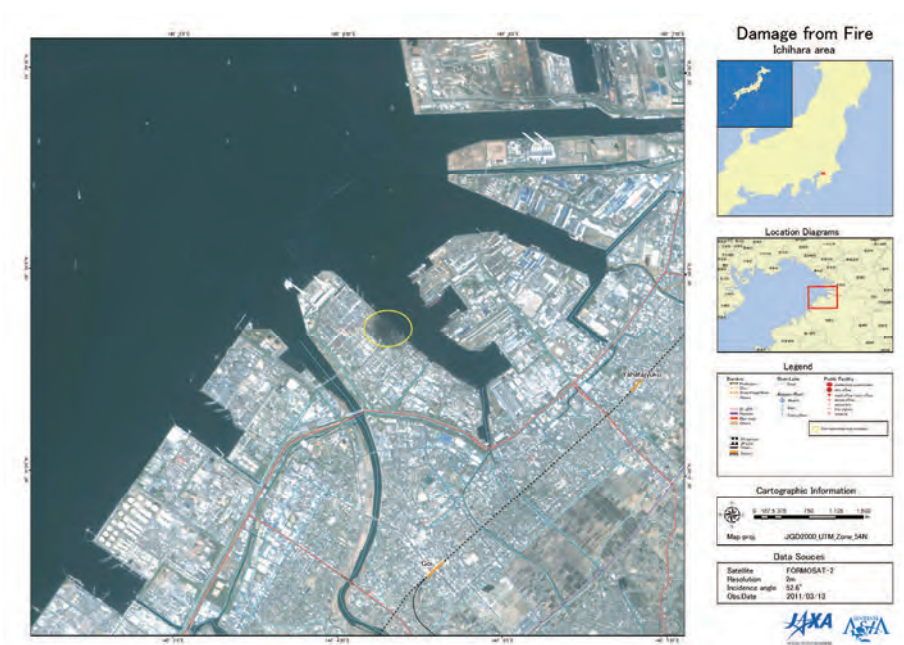


Figure 2.1-28 Satellite topographical image showing the area of the oil refinery fire in Ichihara City, Chiba